

RESEARCH

Open Access



# Synthesis and biological assessment of novel 4*H*-chromene-3-carbonitrile derivatives as tyrosinase inhibitors

Mohammad Azimi<sup>1</sup>, Zahra Najafi<sup>1</sup>, Asrin Bahmani<sup>1</sup>, Gholamabbas Chehardoli<sup>1\*</sup> and Aida Iraj<sup>2,3\*</sup>

## Abstract

Excessive activity of the tyrosinase enzyme during melanogenesis results in hyperpigmentation in the skin. To address this issue, there is a need to develop effective tyrosinase inhibitors as a treatment for hyperpigmentation. In this study, we synthesized some novel 4*H*-chromene-3-carbonitrile compounds (**6a-o**) and assessed their inhibitory activities against tyrosinase, comparing them with kojic acid, which is known as a positive control. Compound **6f** emerged as the most effective inhibitor, with an IC<sub>50</sub> of 35.38 ± 2.12 μM. Kinetic studies of **6f** exhibited competitive inhibition, with  $K_i = 16.15$  μM. Molecular docking studies highlighted the importance of π-π stacking and hydrogen bonding interactions within the binding site. Molecular dynamics simulations showed that the *R*-enantiomer **6f** exhibited superior binding stability compared to the *S*-enantiomer, with a lower standard deviation of RMSD and more persistent interactions with the key active site residues. These findings underscore the potential of the *R*-enantiomer of compound **6f** as a potent tyrosinase inhibitor and provide insights for developing effective treatments for hyperpigmentation and related skin conditions.

**Keywords** Melanogenesis, 4*H*-chromene-3-carbonitrile derivatives, Tyrosinase inhibitors, Molecular docking, Molecular dynamics simulation

## Introduction

Melanogenesis is a crucial biological process that produces melanin, the natural pigment responsible for protecting organisms from sun-induced skin damage. This process is essential for maintaining skin integrity and preventing damage from ultraviolet radiation [1].

While melanin is crucial for protecting the skin from harmful sun rays, excessive melanin production is a common concern for many individuals, especially in conditions like melasma and lentiginosis [2].

Tyrosinase is a key enzyme in melanin production, catalyzing the hydroxylation of *L*-tyrosine to form *L*-dihydroxyphenylalanine (*L*-Dopa), which is then oxidized to create dopaquinone. This dopaquinone undergoes a series of reactions that lead to melanin formation [3, 4]. Additionally, in the early stages of melanogenesis,

\*Correspondence:

Gholamabbas Chehardoli  
cheh1002@gmail.com

Aida Iraj  
iraji@sums.ac.ir

<sup>1</sup>Department of Medicinal Chemistry, School of Pharmacy, Medicinal Plants and Natural Products Research Center, Hamadan University of Medical Sciences, Hamadan, Iran

<sup>2</sup>Department of Persian Medicine, School of Medicine, Research Center for Traditional Medicine and History of Medicine, Shiraz University of Medical Sciences, Shiraz, Iran

<sup>3</sup>Stem Cells Technology Research Center, Shiraz University of Medical Sciences, Shiraz, Iran



© The Author(s) 2024. **Open Access** This article is licensed under a Creative Commons Attribution-NonCommercial-NoDerivatives 4.0 International License, which permits any non-commercial use, sharing, distribution and reproduction in any medium or format, as long as you give appropriate credit to the original author(s) and the source, provide a link to the Creative Commons licence, and indicate if you modified the licensed material. You do not have permission under this licence to share adapted material derived from this article or parts of it. The images or other third party material in this article are included in the article's Creative Commons licence, unless indicated otherwise in a credit line to the material. If material is not included in the article's Creative Commons licence and your intended use is not permitted by statutory regulation or exceeds the permitted use, you will need to obtain permission directly from the copyright holder. To view a copy of this licence, visit <http://creativecommons.org/licenses/by-nc-nd/4.0/>.

the enzyme tyrosinase plays a critical role by catalyzing the oxidation of phenol to *o*-quinone, a crucial step in the melanin production pathway [5]. Tyrosinase is a copper-containing enzyme with six key histidine residues in its active site, which are essential for its catalytic function [6]. Disruptions in tyrosinase activity can lead to abnormal pigment production, potentially resulting in excessive melanin production and hyperpigmentation. These conditions are associated with various skin disorders, ranging from benign to potentially serious, such as freckles, age spots, pregnancy spots, melasma, acne, and melanoma, one of the most deadly types of cancer [1]. To address these challenges, researchers have been actively exploring the development of tyrosinase inhibitors, which can regulate melanin production and mitigate related skin issues. Most cosmetics and skin-lightening products function by inhibiting tyrosinase, an enzyme crucial for melanogenesis, which is exclusively produced by melanocytes [7].

In this context, synthetic agents such as quinazolinone [8], isopropylquinazolinone [9], indole [10], and  $\alpha,\beta$ -unsaturated carbonyl compounds [11], thiazolopyrimidine [12] and vanillin-benzylidenehydrazine [13] have been developed as potent tyrosinase inhibitors. One of the most well-known examples is kojic acid, an FDA-approved tyrosinase inhibitor, which has been widely reported for its use in reducing melanin production. However, kojic acid's clinical use is often limited by skin irritation and chemical instability, leading to side effects [14]. To overcome these drawbacks, modifications of kojic acid have been pursued. For instance, kojic acid conjugated with thio-quinazolinones has shown enhanced tyrosinase inhibitory activity and significant potency against the B16F10 melanoma cell line, effectively reducing melanin content (Fig. 1, compound A) [8]. Similarly, kojic acid derivatives linked to an amino-pyridine moiety have emerged as potent tyrosinase inhibitors. The kojic moiety plays a crucial role in these interactions, forming coordination bonds with two  $\text{Cu}^{2+}$  ions, hydrogen bonds with His279, and engaging in  $\pi$ - $\pi$  stacking interactions with His263 (Fig. 1, compound B) [15]. One such compound exhibited high inhibitory activity against tyrosinase with an  $\text{IC}_{50}$  of 26.5  $\mu\text{M}$  (compound C) [16].

Further structural modifications of the pyran ring embedded in kojic acid derivatives have also been explored, resulting in the development of chromene-based analogs with potent tyrosinase inhibitory effects (Fig. 1, compounds D-G) [17, 18]. These analogs demonstrate that the pyran core structure in the kojic acid derivatives is a crucial feature for tyrosinase inhibition. Recent advancements include novel kojic acid-fused 2-amino-3-cyano-4H-pyrans, which have been evaluated in both *R* and *S* isomeric forms. The compound H exhibited mixed-type inhibition with a  $K_i$  of 7.57  $\mu\text{M}$

and demonstrated superior interactions compared to the *S*-enantiomer [17]. The kojopyran moiety was shown to form hydrogen bonds with Gly281 (2.52 Å) and additional critical interactions with Phe264, His244, and metal chelation with Cu, underscoring its potential as a robust tyrosinase inhibitor [19].

Continuing our ongoing investigations into bioactive heterocycles [20–22], with a particular focus on those that inhibit tyrosinase [19, 23, 24], we have designed a new series of 4H-chromene-3-carbonitrile derivatives in this study. The methoxy linker was closed following the methodology of Najafi et al., with various groups substituted at the  $R_1$  and  $R_2$  moieties. These derivatives were subsequently evaluated for their in-vitro enzyme inhibitory activities. Additionally, we conducted kinetic studies, molecular docking, and molecular dynamics simulations on the most potent compound to further elucidate its mechanism of action.

## Results and discussion

### Chemistry

The synthesis of the products 6a-o involved multiple stages, as detailed in Scheme 1. Initially, benzyloxy-benzaldehydes 3a-c were synthesized via a nucleophilic reaction. This reaction occurred between 4-hydroxy-benzaldehydes or vanillin (1a-b) and benzyl halide derivatives (2a-h), using potassium carbonate in DMF at ambient temperature. Subsequently, a multicomponent synthesis involving benzyloxy-benzaldehydes 3a-o, dimedone 4, and malononitrile 5 was performed in acetonitrile (5 mL), utilizing triethylamine as a catalyst under reflux conditions. This process successfully produced the desired compounds 6a-o with satisfactory yields (52–69%). The structures of all newly synthesized 4H-chromene-3-carbonitrile derivatives was confirmed using NMR, Mass, and IR spectroscopy.

The mechanism of 4H-chromene-3-carbonitrile ring formation is shown in Scheme 2. Initially, intermediate VII is generated through the condensation of one equivalent of dimedone with an aldehyde. Subsequently, the malononitrile reacts with intermediate VII and after removing  $\text{H}_2\text{O}$ , the 4H-chromene-3-carbonitrile ring is formed.

### Biological study

#### *In vitro* tyrosinase inhibitory activity

The anti-tyrosinase properties of these 4H-chromene-3-carbonitrile derivatives (6a-o) were assessed by comparing their activity against mushroom tyrosinase to that of kojic acid, which served as a positive control (Table 1). The most potent derivatives in this set were 6e and 6f, with  $\text{IC}_{50}$  values of  $39.09 \pm 0.34 \mu\text{M}$  and  $35.38 \pm 2.12 \mu\text{M}$ , respectively.

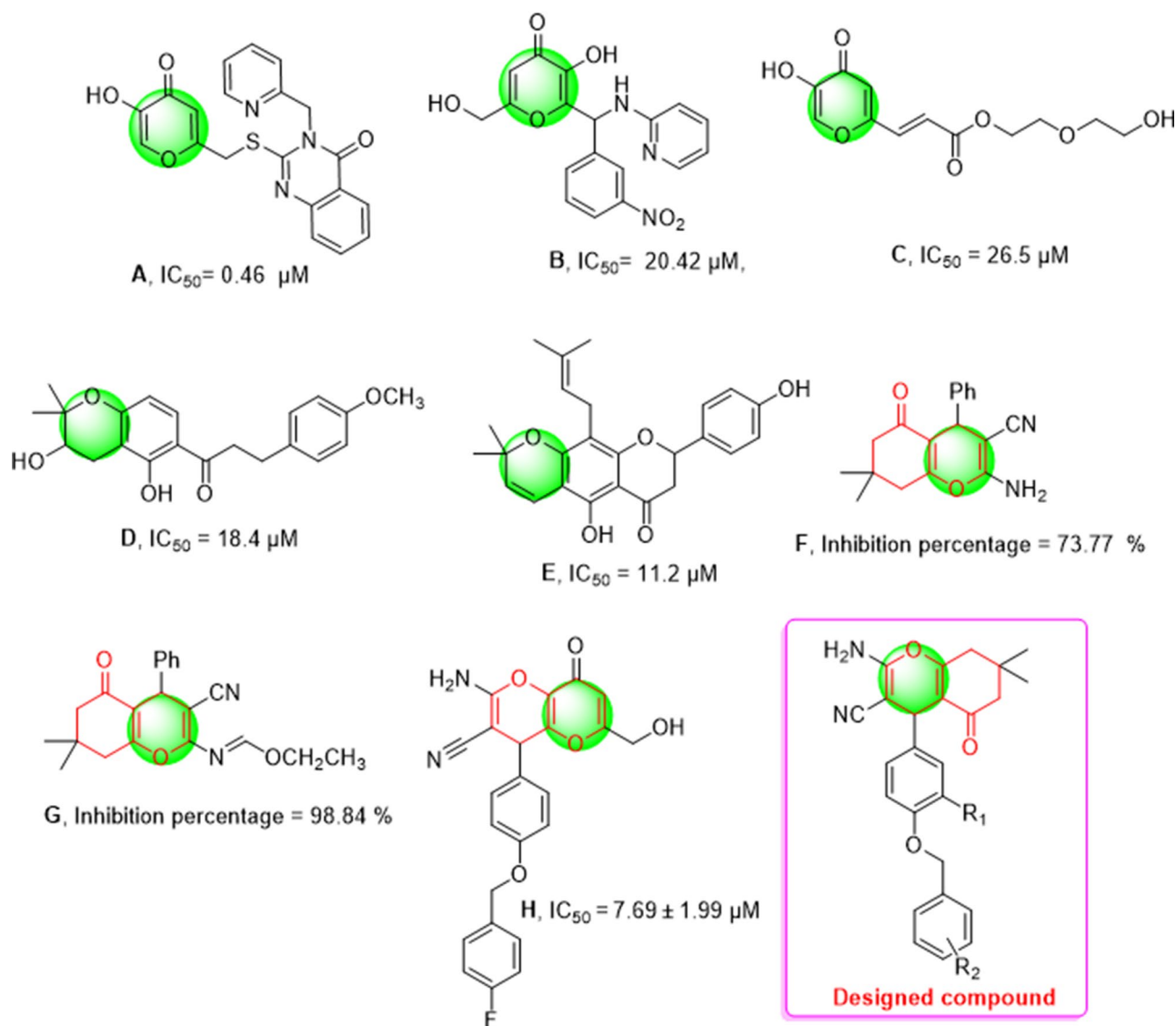
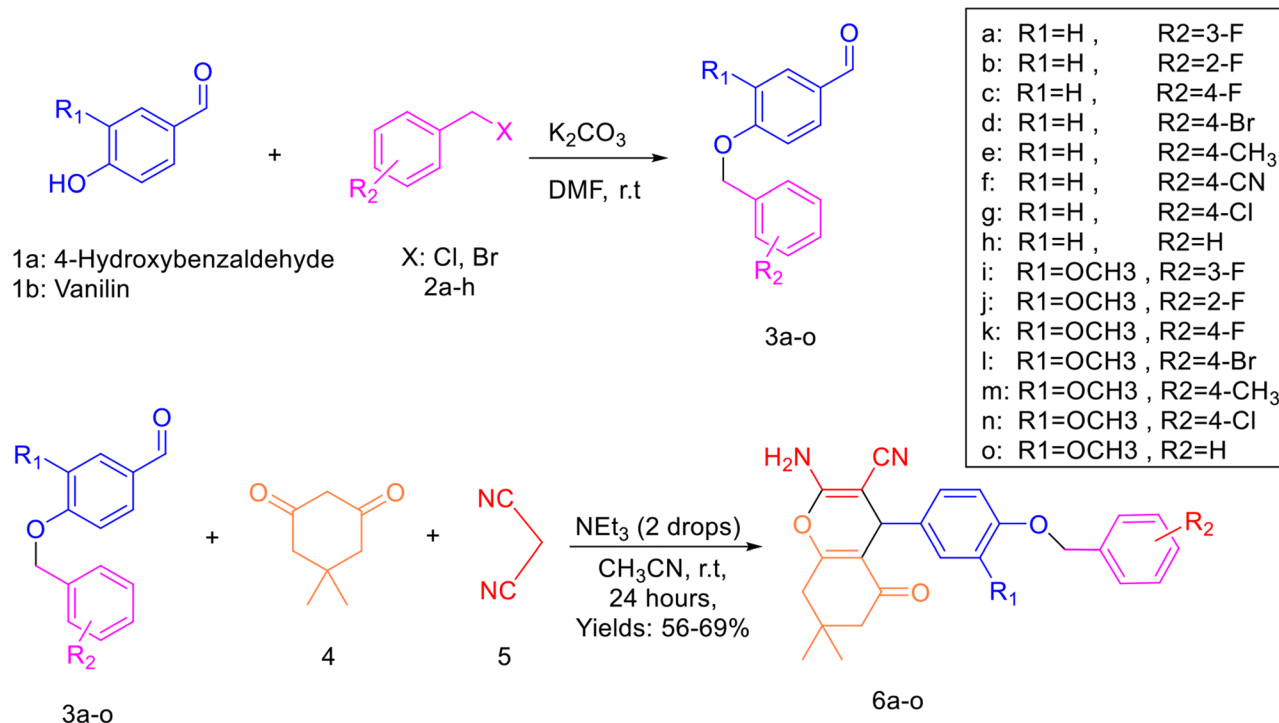


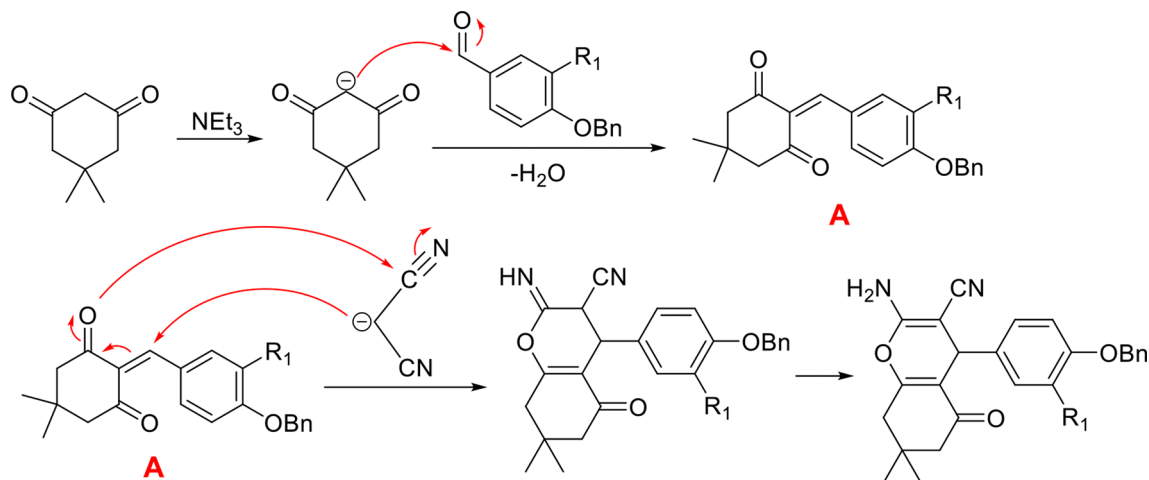
**Fig. 1** Designed pyran derivatives based on compounds containing pyran and chromene scaffolds

To properly evaluate the structure-activity relationship (SAR), the derivatives were divided into two groups based on the  $R_1$  substitution. Among compounds **6a-h** bearing  $R_1 = \text{H}$ , compound **6h**, as an unsubstituted derivative, exhibited weak potency against tyrosinase. To improve potency, different moieties were substituted at the  $R_2$  position. Evaluation of derivatives bearing fluorine at the  $R_2$  position showed the following order of activity: **6b** ( $R_2 = 2\text{-F}$ ) > **6a** ( $R_2 = 3\text{-F}$ ) and compound **6c** ( $R_2 = 4\text{-F}$ ) exhibited no activity. The lack of activity in **6c** indicates that the 4-fluoro substitution might create steric hindrance or disrupt essential interactions within the enzyme's active site. Next, to improve activity at the *para* position, derivatives **6d** ( $R_2 = 4\text{-Br}$ ) and **6g** ( $R_2 = 4\text{-Cl}$ ) were synthesized, which demonstrated improved potency compared to **6c**. The improved activity of **6d** and

**6g** suggests that the optimal size and electronegativity of bromine and chlorine facilitate better interactions with the enzyme and enhance potency. Notably, the presence of a methyl group as an electron-donating group at the *para* position significantly increased the potency, with an  $IC_{50}$  value of  $39.09 \pm 0.34 \mu\text{M}$ . The increased potency of **6e** ( $R_2 = 4\text{-CH}_3$ ) may be attributed to the electron-donating effect of the methyl group, which could enhance the binding affinity by increasing the electron density on the aromatic ring and facilitating stronger interactions with the active site residues. Following this, derivative **6f** ( $R_2 = 4\text{-CN}$ ) showed the most potent inhibition, displaying an  $IC_{50}$  value of  $35.38 \pm 2.12 \mu\text{M}$ . The high potency of **6f** can be explained by the presence of the cyano group, which creates a favorable environment for binding to the enzyme's active site through hydrogen bonding or dipole



**Scheme 1** Synthesis of 4H-chromene-3-carbonitrile derivatives **6a-o**



**Scheme 2** Mechanism of 4H-chromene-3-carbonitrile ring formation

interactions. Also, it can participate in  $\text{Cu}^{2+}$  interaction with the binding site of the enzyme.

Next, derivatives **6i-o** containing methoxy at the  $R_1$  position were synthesized. Fluorine derivatives at the  $R_2$  position exhibited that compound **6k** ( $R_2=4\text{-F}$ ) recorded better results compared to **6i** ( $R_2=3\text{-F}$ ) and **6j** ( $R_2=2\text{-F}$ ). The better activity of **6k** suggests that the 4-fluoro substitution is more favorable when a methoxy group is present at  $R_1$ , likely due to an optimal electronic and steric fit in the enzyme's active site. This trend differs from that seen in compounds **6a-c** bearing H at  $R_1$ . It seems that the presence of a methoxy group at the  $R_1$  position results in

an orientation that made a substitution at the *para* position more favorable compared to *meta* and *ortho*.

However, similar to the previous set, **6n** ( $R_2=4\text{-Cl}$ ) was more potent than **6l** ( $R_2=4\text{-Br}$ ). This suggests that chlorine is more compatible with the enzyme's active site than bromine when a methoxy group is present at  $R_1$ , possibly due to its smaller size and favorable electronegativity. However, these derivatives exhibited lower activity compared to their counterparts in the  $R_2=H$  set. Similarly, the evaluation of **6m**, which bears an electron-donating group, recorded significantly lower activity compared to **6e**. In contrast, derivative **6o**, with no substitution at the

Entry	compounds	R <sub>1</sub>	R <sub>2</sub>	% Inhibition at 40 μM <sup>a</sup>	% Inhibition at 10 μM <sup>a</sup>	IC <sub>50</sub> (μM)
1	6a	H	3-F	13.63 ± 1.81	1.07 ± 0.01	-
2	6b	H	2-F	16.05 ± 1.10	6.03 ± 0.51	-
3	6c	H	4-F	-	5.77 ± 1.60	-
4	6d	H	4-Br	28.74 ± 2.69	19.46 ± 2.43	-
5	6e	H	4-CH <sub>3</sub>	50.67 ± 0.69	4.16 ± 0.32	39.09 ± 0.34
6	6f	H	4-CN	61.38 ± 12.28	17.68 ± 1.11	35.38 ± 2.12
7	6g	H	4-Cl	36.04 ± 5.61	11.87 ± 1.51	-
8	6h	H	H	2.97 ± 0.09	Not Active	-
9	6i	OCH <sub>3</sub>	3-F	24.46 ± 2.27	8.58 ± 0.99	-
10	6j	OCH <sub>3</sub>	2-F	10.40 ± 0.19	2.92 ± 0.07	-
11	6k	OCH <sub>3</sub>	4-F	31.53 ± 3.55	8.31 ± 0.36	-
12	6l	OCH <sub>3</sub>	4-Br	23.02 ± 2.82	5.15 ± 0.11	-
13	6m	OCH <sub>3</sub>	4-CH <sub>3</sub>	30.65 ± 5.60	17.97 ± 1.86	-
14	6n	OCH <sub>3</sub>	4-Cl	31.00 ± 2.36	17.70 ± 1.19	-
15	6o	OCH <sub>3</sub>	H	22.56 ± 2.14	5.24 ± 0.23	-
<b>Kojic acid<sup>b</sup></b>						23.64 ± 2.56

<sup>a</sup> Data presented here is the mean ± S.E

<sup>b</sup> Positive control.

**Table 1** Inhibitory activities of the new compounds **6a-o** against tyrosinase<sup>a</sup>

R<sub>2</sub> position, exhibited better activity than its **6a** counterpart. Overall, it can be suggested that, in the presence of the bulky methoxy group at R<sub>1</sub>, which increases the electron density on the central benzene ring, the absence of substitution at R<sub>2</sub> or the presence of a small group reduces steric hindrance. This reduction in steric hindrance allows for better accommodation within the enzyme's active site and improves the potency.

#### Kinetic study

The mechanism and type of inhibition were elucidated through comprehensive kinetic studies. To determine the mode of enzyme inhibition, we performed a Lineweaver-Burk plot analysis using the most effective derivative, compound **6f** (Fig. 2). The Lineweaver-Burk plot, which

graphs 1/V against 1/[S], was utilized to demonstrate the inhibition of tyrosinase by **6f** at various concentrations of both the inhibitor (**6f**) and the substrate (L-Dopa). In this analysis,  $K_m$  refers to the Michaelis-Menten constant, while  $V_{max}$  denotes the maximum reaction velocity.

The data analysis revealed that the  $V_{max}$  of the enzyme remained unchanged, while the  $K_m$  values increased with higher concentrations of compound **6f**. This pattern indicates that compound **6f** acts as a competitive inhibitor. The plot of the slope of the lines *versus* different concentrations of **6f** provided an estimate of the inhibition constant,  $K_i = 16.15 \mu\text{M}$ .

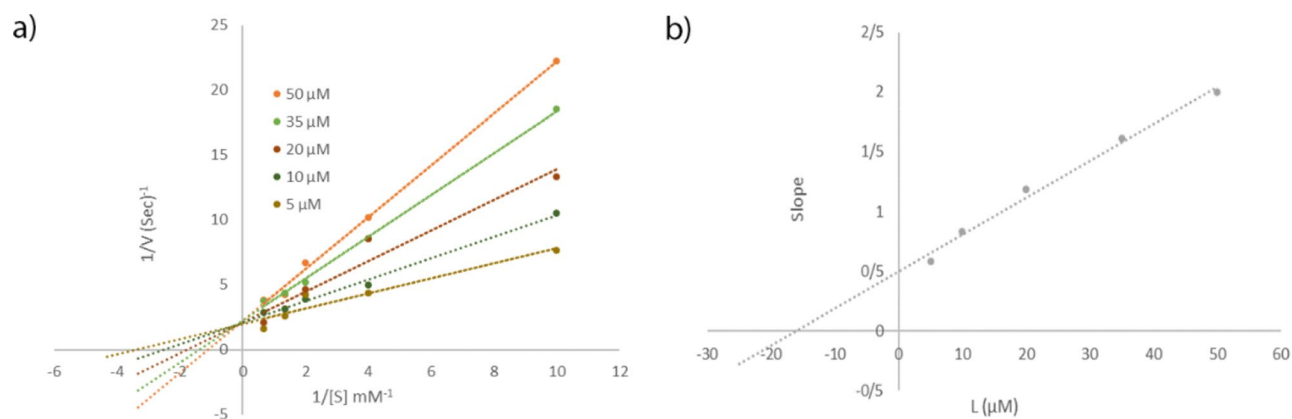


**Fig. 2** Kinetic study of compound **6f** against tyrosinase. **(a)** The Lineweaver–Burk plot in the absence and presence of different concentrations of compound **6f**; **(b)** The secondary plot of the slope of lines and various concentrations of compound **6f**

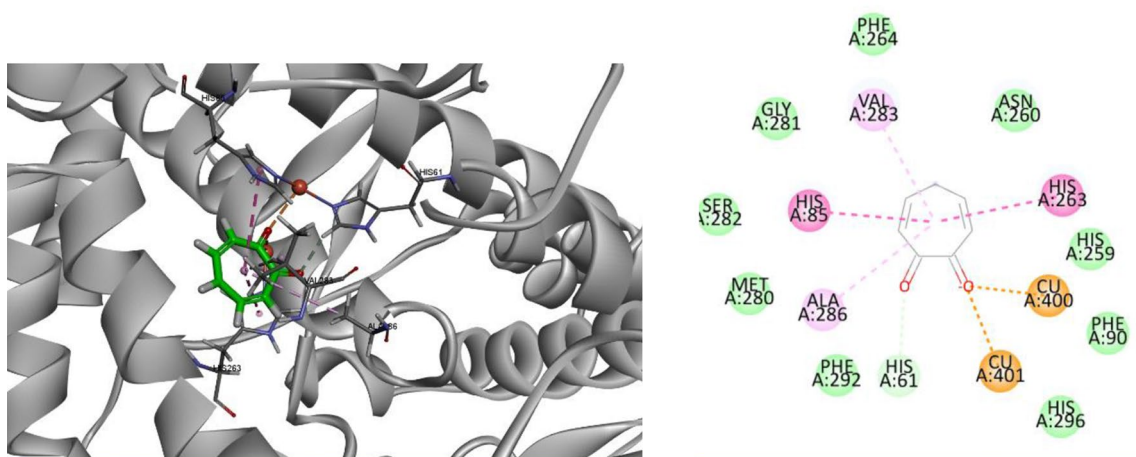


**Fig. 3** 3D and 2D interaction of tropolone in complex with tyrosinase

### Molecular docking study

To elucidate the molecular interactions between compound **6f** and the tyrosinase enzyme, docking studies were conducted. Key amino acids in the active site of the tyrosinase enzyme (PDB ID: 2Y9X) are His259, His263, Phe90, His85, Cys83, His61, His94, Phe292, His296, Val283, and Phe264 [25]. Before performing the molecular docking study, the docking protocol was validated to ensure accuracy. Tropolone, the crystallographic ligand, was docked into the active site of tyrosinase, and the Root Mean Square Deviation (RMSD) was determined by comparing the best docking pose with the crystallographic ligand. The RMSD value was found to be less than 2 Å, indicating reliable accuracy of the docking protocol. Tropolone exhibited two interactions with both  $\text{Cu}^{2+}$  cofactors, as well as a hydrogen bond with His61. Additionally, it showed two  $\pi$ - $\pi$  stacking interactions with His85 and His263, and two  $\pi$ -alkyl interactions with Val283 and Val286 (Fig. 3).

Compound **6f**, selected as the most effective inhibitor based on in vitro tyrosinase inhibitory assay, was

synthesized as a racemic mixture, and thus, both the *R* and *S* isomers were evaluated in the docking studies.

The *S*-isomer of compound **6f** exhibited a predicted free energy of binding of -5.27 kcal/mol when docked into the active site of tyrosinase. This binding energy suggests that the *S*-isomer may interact strongly with the enzyme. This isomer established a hydrogen bond with Val283 through the oxygen linked to the benzyl group. Furthermore, the phenyl ring connected to the pyran moiety displayed  $\pi$ - $\pi$  stacking interactions with Phe264, and the benzyl group exhibited  $\pi$ - $\pi$  stacking interactions with the amino acid residue His263.

Regarding the *R*-isomer, the calculated free energy of binding within the active site of tyrosinase was -5.44 kcal/mol. The *R*-isomer forms  $\pi$ - $\pi$  stacking interactions with His263 through its benzyl group. These interactions play a vital role in stabilizing the ligand in the active site and positioning it optimally for enzyme inhibition. The docking study highlights the importance of  $\pi$ - $\pi$  stacking and hydrogen bonding interactions in the binding of compound **6f** to tyrosinase enzyme.

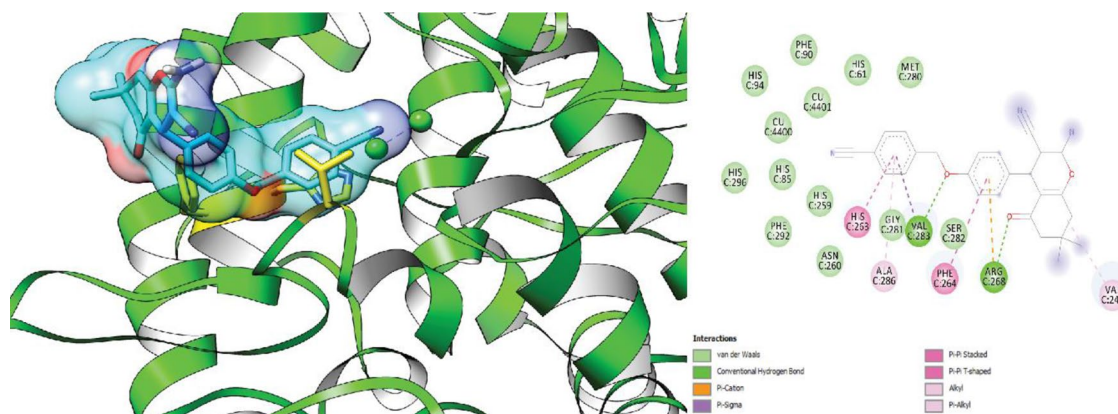


**Fig. 4** 3D and 2D interaction of the *S*-enantiomer of compound **6f** in complex with tyrosinase

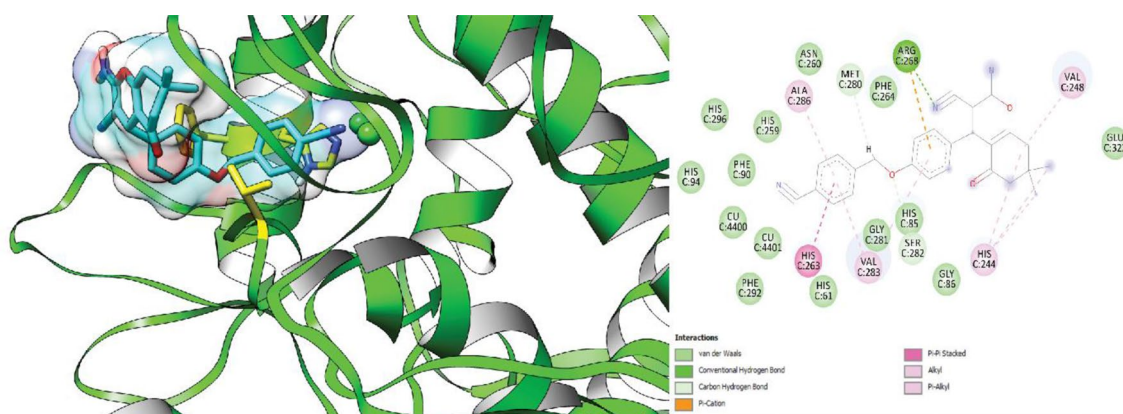


**Fig. 5** 3D and 2D interaction of the *R*-enantiomer of compound **6f** in complex with tyrosinase

After conducting the molecular docking study, we utilized the bootstrapping method to analyze the confidence interval for each isomer, as the calculated energy values for both the *R* and *S* isomers were very close (Figs. 4 and 5). The 95% confidence intervals were calculated and found to be (-5.43, -5.35) for the *R* isomer and (-5.41, -5.20) for the *S* isomer. The non-overlapping confidence intervals suggest that the *R*-isomer, which exhibits a more favorable estimated free energy of binding, represents the best docking outcome.

Also, the molecular docking study of all derivatives was also performed and the results are summarized in table S1. Compounds with fluorine substitutions (**6a-c**) exhibit binding energies ranging from -4.681 to -4.893 kcal/mol. The electron-withdrawing nature of fluorine reduces the electron density on the aromatic rings, which weakens both  $\pi$ - $\pi$  stacking and Pi-Alkyl interactions, possibly explaining the reduced anti-tyrosinase activity of these compounds. In contrast, bromine substitutions (**6d, 6L**) introduce steric hindrance due to bromine's large size, but they compensate with stabilizing interactions through metal-acceptor coordination with copper,  $\pi$ - $\pi$  stacking, and hydrogen bonds. These interactions result in moderate binding affinities, with free energies

of -5.001 and -5.136 kcal/mol. Chlorine substitutions (**6g, 6n**) improve binding affinity due to chlorine's smaller size, which reduces steric hindrance and enhances stability through Pi-Alkyl and metal-acceptor interactions with copper. Methyl substitutions (**6e, 6m**) serve as electron donors, significantly strengthening Pi-Alkyl and Pi-Pi stacking interactions. Compound **6e**, with the strongest binding affinity (-7.306 kcal/mol), achieves this through extensive interactions, including multiple hydrogen bonds and  $\pi$ - $\pi$  stacking. The cyano substitution (**6f**) shows a strong binding affinity (-5.44 kcal/mol) due to hydrogen bonds and Pi-Alkyl interactions, with cyano's electron-withdrawing nature stabilizing the interactions within the enzyme's active site.

Overall, it can be understood that hydrogen bonds are notably observed in compound **6e**, which forms bonds with His85 and Asn260, and in compound **6f**, where hydrogen bonds form with Arg268 *via* the cyano group.  $\pi$ - $\pi$  stacking interactions are evident in compound **6e**, where the phenoxy and substituent groups stack with His85 and His263, while compound **6f** exhibits stacking interactions with His263 for both the substituted moiety and phenoxy groups. For Pi-Alkyl interactions, compound **6e** shows a methyl group on the substituted

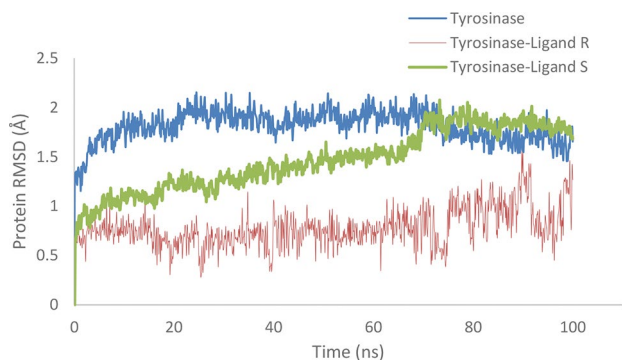


**Fig. 6** RMSD of tyrosinase (in blue), the complex of tyrosinase with the *R*-enantiomer **6f** (in red), complex of tyrosinase with *S*-*S*-enantiomer **6f** (in green) over a molecular dynamics simulation time of 100 ns

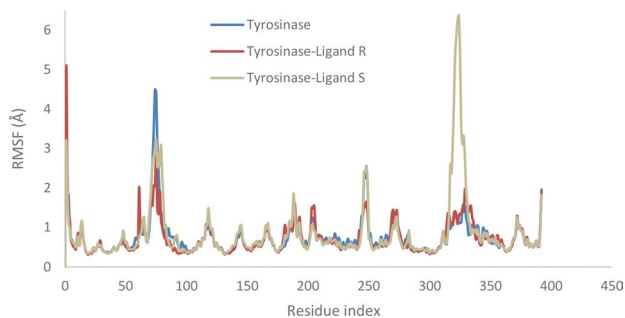


**Fig. 7** RMSF of tyrosinase (in blue), complex of tyrosinase with the *R*-enantiomer **6f** (in orange), complex of tyrosinase with *S*-enantiomer **6f** (in gray) for a 100 ns molecular dynamics simulation time

moiety interacting with Phe264, while both the phenoxy and substituted moiety interact with Val283 and Ala286. In compound **6f**, methyl groups on the tetrahydro-5 H-chromen-5-one core interact with His244, while the tetrahydro-5 H-chromen-5-one, phenoxy, and substituted moiety engage in Pi-Alkyl interactions with Val248, His244, Val283, and Ala286.

### Molecular dynamic simulation

To further investigate the stability and interaction of the *R* and *S* isomers of compound **6f** with tyrosinase enzyme, we accomplished molecular dynamics (MD) simulations. These simulations were performed over 100 nanoseconds to evaluate the dynamic behavior and binding stability of the isomers within the enzyme's active site. The standard deviation of the root mean square deviation (RMSD) values, which indicate fluctuations in the enzyme's three-dimensional structure, was 0.19 for the *R* isomer and 0.31 for the *S* isomer (Fig. 6). Additionally, the average RMSD values for the *R* and *S* isomers were 0.77 and 1.46, respectively. The lower standard deviation observed for the *R* isomer suggests a more stable enzyme conformation during the simulation period compared to that of the *S* isomer.

Figure 7 illustrates that the root mean square fluctuation (RMSF) values for key residues in the active site including His259, His263, Phe90, His85, Cys83, His94, Phe292, His296, Val283, and Phe264 were lower in the presence of the *R* isomer compared to the *S* isomer. This observation suggests that the *R* isomer enhances stability and decreases flexibility in these residues, indicating a more effective binding interaction.

The *R* isomer demonstrated sustained interactions with the active site, which are crucial for ensuring binding stability. Notably, the cyano (CN) group of the benzyl ring of the *R* isomer engaged in chelation with the copper ion in the active site for 56% of the simulation period (Fig. 8b). This interaction also affected the coordination of the copper ions with adjacent amino acids, including His259, His263, His296, and Glu256. Among these, the interaction between the benzyl moiety and His263 was particularly significant, persisting for 92% of the simulation time. This interaction seems crucial for determining both the orientation and effectiveness of the *R* enantiomer within the binding site.

As shown in Fig. 8a, the *R* enantiomer demonstrated a notably greater number of interactions with the enzyme's active site throughout the simulation period. These interactions play a crucial role in enhancing the stability of the enzyme-ligand complex, as supported by the RMSD results. In the case of the *S* enantiomer, the phenyl attached to the pyran moiety of the *S* isomer interacted with His85 for 23% of the simulation time which indicates that the *S* enantiomer does not interact as effectively with other key residues compared to the *R* enantiomer (Fig. 9).

The MD simulations indicate that the *R* isomer of compound **6f** exhibits better binding stability and interaction with the tyrosinase enzyme when compared to the *S* isomer. The *R* isomer's enhanced stability and effective interactions highlight its potential as a more potent inhibitor of tyrosinase.

### Drug-likeness prediction

The concept of drug-likeness was introduced by Lipinski, known as the Rule of Five. This rule outlines specific physicochemical parameters that are typically associated with orally active drugs. The criteria include: a molecular weight (MW) of no more than 500 daltons, a maximum of 10 hydrogen bond acceptors (HBA), a maximum of 5 hydrogen bond donors (HBD), a lipophilicity index (logP) not exceeding 5, up to 10 rotatable bonds (RBC), and a polar surface area (PSA) of 140 Å<sup>2</sup> or less [26]. To assess these parameters, two online tools, pkCSM and SwissADME, were utilized [27, 28]. Compounds **6e** and **6f** were identified as the most promising antityrosinase agents and were selected for further evaluation of their physicochemical properties. The data presented in Table 2 demonstrate that two lead compounds

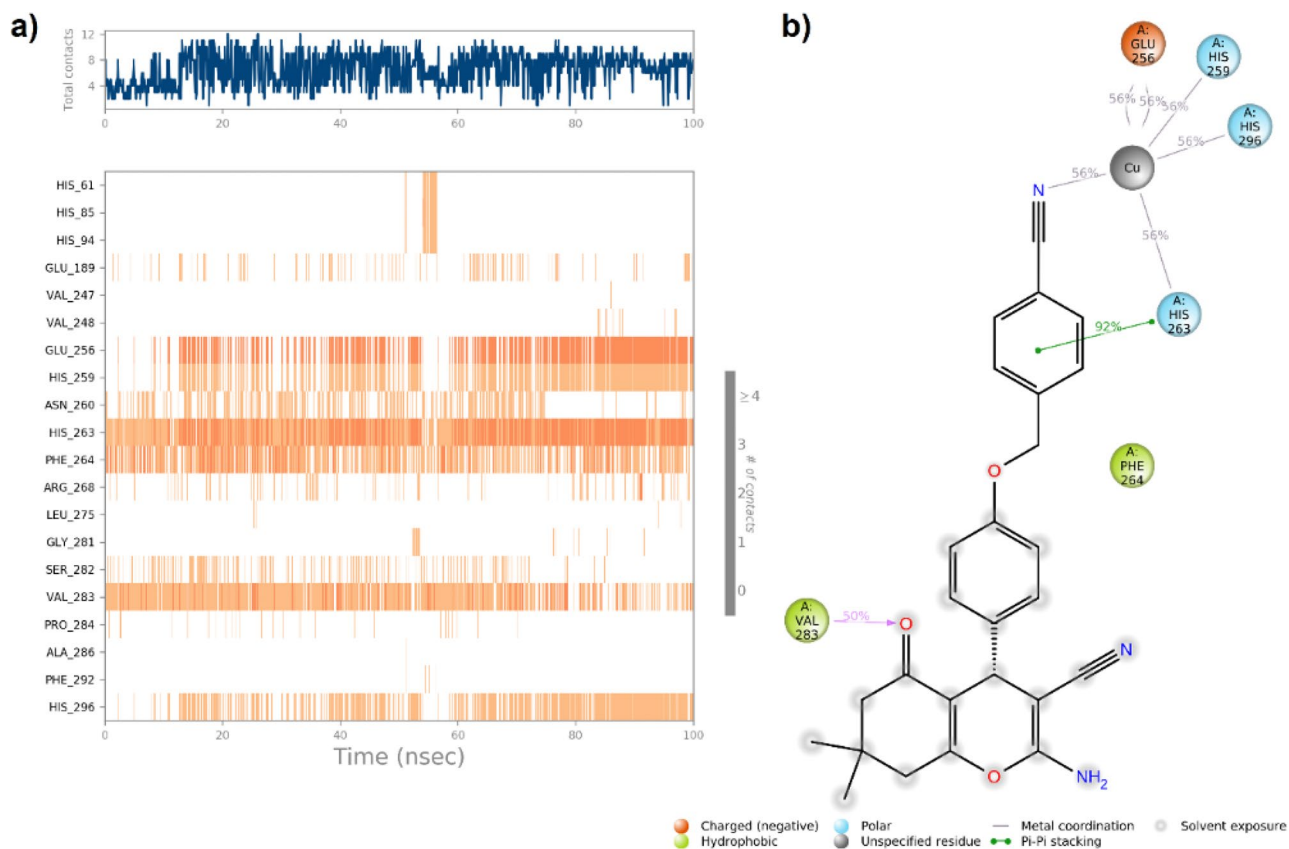


**Fig. 8** (a) A timeline representation of the interactions and contacts; (b) Protein residue interactions with *R*-enantiomer atom

successfully met the criteria outlined in Lipinski's rule of five.

### Prediction of ADMET properties

The ADMET (Absorption, Distribution, Metabolism, Excretion, and Toxicity) properties of compounds **6e** and **6f** were predicted using pkCSM, SwissADME, and Pro-Tox online servers [27–29]. Compound **6e** demonstrated a blood-brain barrier (BBB) permeability (Log BB) of -0.227, excellent intestinal absorption at 93.38%, and a steady-state volume of distribution (VD<sub>ss</sub>) of 0.286, indicating moderate distribution characteristics. It is a substrate and inhibitor for CYP3A4 as well as an inhibitor of CYP2C9 and CYP2C19 (Table 3). This suggests that drug interactions should be carefully considered, particularly with drugs that have narrow therapeutic indices that are metabolized by these enzymes. Furthermore, **6e** is neither a substrate nor an inhibitor for CYP2D6, reducing the risk of interactions with other drugs in this metabolic pathway. Notably, **6e** is not a substrate for renal OCT2, which means that compound **6e** is unlikely to be involved in transporter-mediated renal drug-drug interactions and may have a favorable safety profile concerning nephrotoxicity. In addition, compound **6e** does not pose risks of cytotoxicity, skin sensitization, or hERG1 inhibition.

Compound **6f** showed a Log BB of -0.133, intestinal absorption of 100%, and a VD<sub>ss</sub> of 0.140 log L/kg, indicating moderate distribution. Similarly, it shares metabolic, excretion, and toxicity profiles similar to those of **6e**. These ADMET profiles indicate that both compounds have promising pharmacokinetic properties, supporting their potential as safe and effective therapeutic agents [30, 31].

### Pan-assay Interference compounds (PAINS) filters

Pan-Assay Interference Compounds (PAINS) represent a significant challenge in medicinal chemistry and high-throughput screening (HTS) due to their tendency to produce false positive results in biological assays. These compounds often bind nonspecifically to multiple targets, leading to misleading outcomes that can divert efforts away from more promising drug candidates. Identifying and excluding PAINS early in the drug discovery process is crucial to avoid wasting time and resources on compounds that are unlikely to lead to successful therapeutics [31–33]. In this study, compounds **6e** and **6f** were subjected to PAINS screening to evaluate their potential for producing false-positive results. Both compounds **6e** and **6f** showed no PAINS alerts in the screenings. This outcome suggests that these compounds do not possess

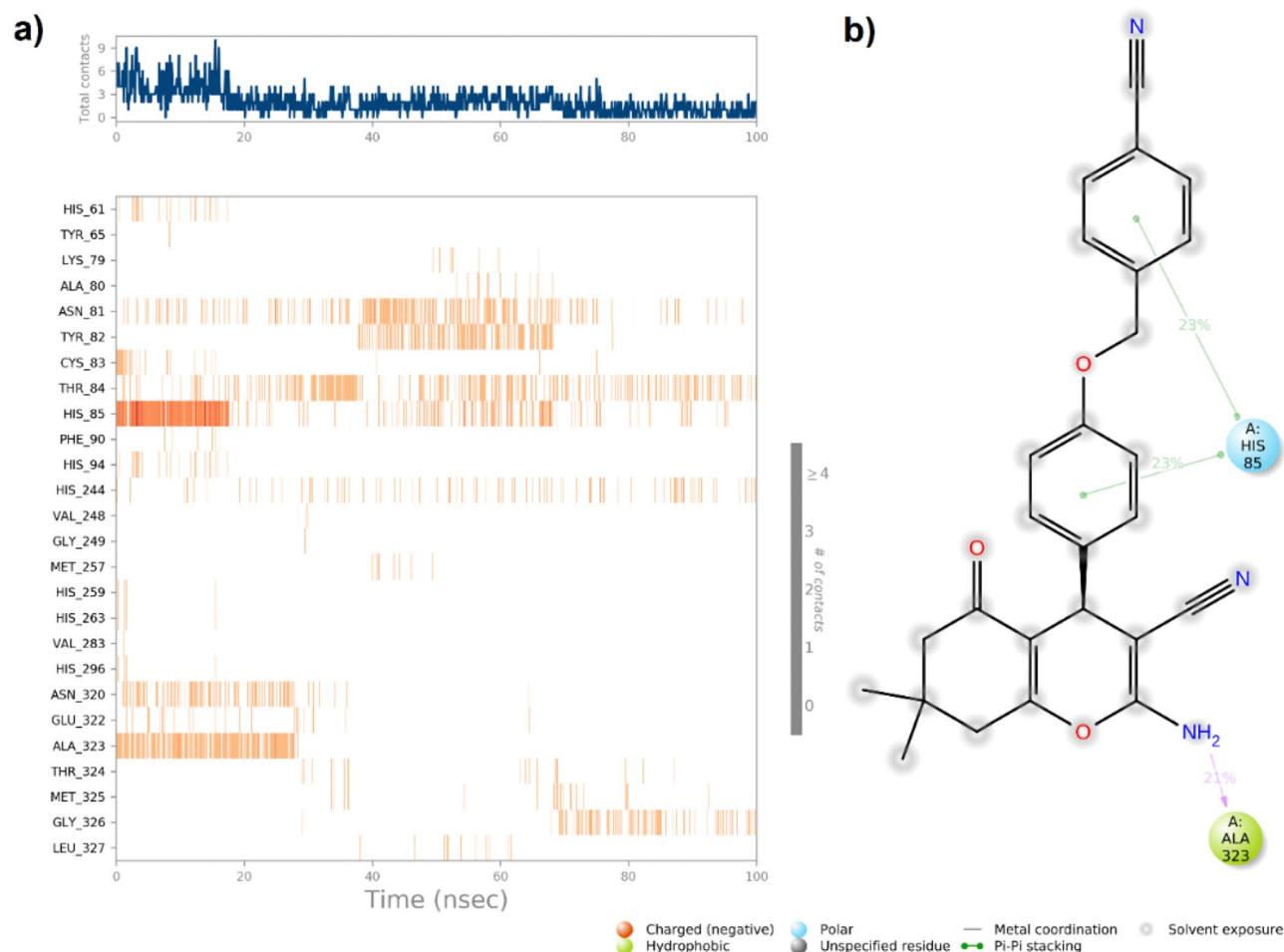


**Fig. 9** (a) A timeline representation of the interactions and contacts; (b) Protein residue interactions with *S*-enantiomer atom

**Table 2** Physicochemical properties of the selected compounds (**6e**, **6f**)

Compound	TPSA	RBC	Log <i>P</i>	HBD	HBA	MW
<b>6e</b>	85.34	4	3.64	1	4	414.50
<b>6f</b>	109.13	4	3.45	1	5	425.48

Abbreviations: MW, molecular weight; HBA, number of H-bond acceptors; HBD, number of H-bond donors; Log *P*, the octanol-water partition coefficient; RBC, rotatable bond count; TPSA, topological polar surface area

the promiscuous binding characteristics typically associated with PAINS; therefore, they are unlikely to interfere with the biological assay results through known nonspecific interactions. The absence of PAINS alerts for compounds **6e** and **6f** is a positive indication of their specificity and potential as viable drug candidates. By passing these initial PAINS filters, the compounds are less likely to be false positives in the early stages of drug discovery, thereby justifying further investigation into their efficacy and safety profiles. This finding supports the continued development of **6e** and **6f** as potential inhibitors of tyrosinase, with a reduced risk of misleading assay results.

## Conclusion

In conclusion, we successfully synthesized a novel series of 4*H*-chromene-3-carbonitrile derivatives (**6a–o**) and evaluated their inhibitory activity against tyrosinase compared to the standard kojic acid. Among them, compound 2-amino-4-(4-((4-cyanobenzyl)oxy)phenyl)-7,7-dimethyl-5-oxo-5,6,7,8-tetrahydro-4*H*-chromene-3-carbonitrile (**6f**), exhibited the most potent inhibition of tyrosinase with an  $IC_{50}$  value of  $35.38 \pm 2.12 \mu\text{M}$ , indicating a competitive inhibition mechanism. Kinetic studies further clarified the inhibition mechanism, confirming that compound **6f** functions as a competitive inhibitor, as demonstrated by the Lineweaver-Burk plot. Additionally, docking studies revealed significant  $\pi$ - $\pi$  stacking and hydrogen bonding interactions, particularly with His263,

**Table 3** ADMETa prediction of the selected compounds **6e** and **6f**

Compound	Absorption		Distribution		Metabolism		Excretion				Toxicity		
	BBB permeability (Log BB)	Intestinal absorption (%Absorbed)	VDss (log L/Kg)	VDss (log L/Kg)	CYP3A4 substrate	CYP3A4 Inhibitor	CYP2C9 inhibitor	CYP2C19 inhibitor	CYP2D6 Substrate	CYP2D6 inhibitor	Renal OCT2 substrate	Skin Sensitization	hERG1 inhibitor
<b>6e</b>	-0.227	93.388	0.286	0.286	Yes	Yes	Yes	Yes	No	No	No	No	No
<b>6f</b>	-0.133	100	0.140	0.140	Yes	Yes	Yes	Yes	No	No	No	No	No

<sup>a</sup>HIA (Human Intestinal Absorption): > 80% is high and < 30% is poor; VDss (steady-state volume of distribution): log L/Kg: > 0.45 is high and < -0.15 is low. A compound is considered to have low skin permeability if it has a logKp > -2.5. PKCSM and SwissADME online servers calculated all data. <sup>b</sup>The software could not predict parameters for these compounds (-)

Val283, and Phe264, which are essential for the ligand's inhibitory potency.

The consistent interactions between the *R*-isomer and key residues, including His263 and the copper ions, underscore its promise as a more effective tyrosinase inhibitor. MD simulations provided further evidence of the *R*-isomer's superior stability within the enzyme's active site. The *R*-isomer exhibited a more stable conformation, as evidenced by a lower standard deviation in RMSD values compared to the *S*-isomer. The consistent interactions between the *R*-isomer and key residues, including His263 and the copper ions. Overall, our findings highlight the potential of the synthesized 4*H*-chromene-3-carbonitrile derivatives as powerful tyrosinase inhibitors. These results offer valuable insights for the design and development of novel tyrosinase inhibitors aimed at treating melanogenesis-related disorders. Continued research and optimization of these compounds may lead to the development of effective therapeutic agents for managing hyperpigmentation and related skin conditions.

## Materials and methods

### Experimental

All chemicals used in the experiments were sourced from Merck and Aldrich. Melting points were measured using a Kofler hot stage apparatus. Nuclear Magnetic Resonance (NMR) spectra, including both <sup>1</sup>H NMR and <sup>13</sup>C NMR, were acquired with Bruker 400 and 300 MHz NMR spectrometers. Infrared (IR) spectra were recorded using a Bruker ALPHA FT-IR spectrometer on KBr disks. Mass spectrometry (MS) data were collected with an Agilent Technologies (HP) mass spectrometer, operating at an ionization potential of 70 eV. <sup>1</sup>H, <sup>13</sup>C NMR were performed by the central lab of Mashhad University of Medical Sciences, Mashhad, Iran, Mass spectra were recorded by the central lab of Tehran University, Tehran, Iran, and IR spectra were recorded by the central lab of Hamadan University of Medical Sciences, Hamadan, Iran.

### Chemistry

#### General procedure for the synthesis of (benzyloxy) benzaldehydes (3a-o)

In a 25 mL round-bottom flask, 1 mmol of hydroxyl benzaldehyde (1a and 1b) and 3 mmol of benzyl halides (2a-h) were dissolved in 3 mL of DMF. To this solution, 1 mmol of potassium carbonate was added, and the mixture was stirred at room temperature for 24 h. The progress of the reaction was monitored using TLC (n-hexane/EtOAc, 4:1). Once completed, the reaction mixture was poured into an ice-water mixture. The resulting precipitates were collected, dried, and utilized in subsequent reactions without additional purification [34].

### General procedure for the synthesis of 4*H*-chromene-3-carbonitrile derivatives (6a-o)

To synthesize the 4*H*-chromene-3-carbonitrile derivatives (6a-o), we began by combining 0.5 mmol of the benzyloxy-benzaldehyde derivatives (3a-o) with 0.5 mmol of dimedone in a 50 ml round-bottom flask. Next, we added 0.6 mmol of malononitrile, two drops of triethylamine, and 4 ml of acetonitrile to the reaction mixture. The mixture was stirred at room temperature for 24 h to ensure the complete reaction. The progress of the reaction was monitored by TLC (n-hexane/EtOAc, 3:2). Once the reaction was finished, the mixture was allowed to cool to room temperature, and the resulting precipitate was filtered out.

2-Amino-4-(4-((3-fluorobenzyl)oxy)phenyl)-7,7-dimethyl-5-oxo-5,6,7,8-tetrahydro-4*H*-chromene-3-carbonitrile (6a)

White solid; Yield: 61%,  $R_f$ =0.45 (n-hexane: EtOAc (60:40)); mp: 210–212 °C.  $^1\text{H}$  NMR (301 MHz,  $\text{DMSO-}d_6$ )  $\delta$  7.46 (td,  $J$ =8.0, 6.0 Hz, 1H), 7.34–7.25 (m, 2 H), 7.22–7.13 (m, 1H), 7.11–7.05 (m, 2 H), 6.99 (s, 2 H), 6.97–6.90 (m, 2 H), 5.10 (s, 2 H), 4.15 (s, 1H), 2.53 (s, 2 H), 2.31–2.07 (m, 2 H), 1.05 (s, 3 H), 0.97 (s, 3 H).  $^{13}\text{C}$  NMR (76 MHz,  $\text{DMSO-}d_6$ )  $\delta$  196.19, 164.27, 162.68, 161.05, 158.89, 157.34, 140.65, 140.55, 137.75, 131.00, 130.89, 128.75, 124.02, 123.98, 120.30, 115.17, 114.97, 114.90, 114.84, 114.56, 113.38, 68.80, 58.91, 50.44, 35.21, 32.27, 28.85, 27.25. Ms m/z (%): 109.1(100), 83.1(15), 66.1(6), 161.1(3), 217.2(12), 243.2(19), 281.1(5.5), 309.2(23), 352.2(10), 419.3(8), 418.3(13.5), 133.1(2). IR (KBr,  $\text{cm}^{-1}$ )  $\nu$ : 3357.4(N-H), 3185.91(C-H aromatic), 2190.61(C $\equiv$ N), 1654.03 (C=O), 1604.96 (C=C aromatic), 1507.98 (C=C aromatic).

2-Amino-4-(4-((2-fluorobenzyl)oxy)phenyl)-7,7-dimethyl-5-oxo-5,6,7,8-tetrahydro-4*H*-chromene-3-carbonitrile (6b).

White solid; Yield: 60%,  $R_f$ =0.42 (n-hexane: EtOAc (60:40)); mp: 214–217 °C.  $^1\text{H}$  NMR (301 MHz,  $\text{DMSO-}d_6$ )  $\delta$  7.57 (td,  $J$ =7.5, 1.8 Hz, 1H), 7.49–7.39 (m, 1H), 7.32–7.21 (m, 2 H), 7.12–7.05 (m, 2 H), 7.00 (s, 2 H), 6.96 (d,  $J$ =8.6 Hz, 2 H), 5.11 (s, 2 H), 4.15 (s, 1H), 2.53 (s, 2 H), 2.30–2.08 (m, 2 H), 1.05 (s, 3 H), 0.97 (s, 3 H).  $^{13}\text{C}$  NMR (76 MHz,  $\text{DMSO-}d_6$ )  $\delta$  196.18, 162.67, 162.49, 159.23, 158.90, 157.39, 137.80, 131.23, 131.18, 130.91, 130.80, 128.77, 125.03, 124.99, 124.45, 124.25, 120.29, 115.99, 115.72, 114.85, 113.40, 63.95, 63.90, 58.93, 50.46, 35.23, 32.26, 28.85, 27.26. Ms m/z (%): 109.1(100), 83.1(10), 66.1(5), 161.1(3), 217.2(13), 243.2(6.5), 281.1(5), 309.2(25), 352.2(5.5), 419.3(4), 418.3(13.5), 133.1(2). IR (KBr,  $\text{cm}^{-1}$ )  $\nu$ : 3357.94(N-H), 3179.32(C-H aromatic), 2187.61(C $\equiv$ N), 1652.44 (C=O), 1604.88 (C=C aromatic), 1508.59 (C=C aromatic).

2-Amino-4-(4-((4-fluorobenzyl)oxy)phenyl)-7,7-dimethyl-5-oxo-5,6,7,8-tetrahydro-4*H*-chromene-3-carbonitrile (6c).

White solid; Yield: 62%,  $R_f$ =0.42 (n-hexane: EtOAc (60:40)); mp: 200–203 °C.  $^1\text{H}$  NMR (301 MHz,  $\text{DMSO-}d_6$ )  $\delta$  7.56–7.45 (m, 2 H), 7.28–7.19 (m, 2 H), 7.10–7.05 (m, 2 H), 6.99 (s, 2 H), 6.97–6.92 (m, 2 H), 5.05 (s, 2 H), 4.14 (s, 1H), 2.53 (s, 2 H), 2.29–2.08 (m, 2 H), 1.05 (s, 3 H), 0.97 (s, 3 H).  $^{13}\text{C}$  NMR (75 MHz,  $\text{DMSO-}d_6$ )  $\delta$  196.18, 163.83, 162.66, 160.61, 158.89, 157.46, 137.64, 133.86, 133.82, 130.50, 130.39, 128.72, 120.30, 115.86, 115.58, 114.94, 113.40, 68.92, 58.93, 50.45, 35.22, 32.26, 28.86, 27.25. Ms m/z (%): 109.2(100), 83.2(7), 66.2(1.5), 161.2(2), 217.2(9), 243.2(4), 281.3(4), 309.3(23), 352.3(8.5), 419.3(5.5), 418.3(21), 133.2(1.5). IR (KBr,  $\text{cm}^{-1}$ )  $\nu$ : 3362.21(N-H), 3179.42(C-H aromatic), 2185.48(C $\equiv$ N), 1653.54(C=O), 1604.07 (C=C aromatic), 1512.66 (C=C aromatic).

2-Amino-4-(4-((4-bromobenzyl)oxy)phenyl)-7,7-dimethyl-5-oxo-5,6,7,8-tetrahydro-4*H*-chromene-3-carbonitrile (6d).

White solid; Yield: 69%,  $R_f$ =0.42 (n-hexane: EtOAc (60:40)); mp: 208–209 °C.  $^1\text{H}$  NMR (301 MHz,  $\text{DMSO-}d_6$ )  $\delta$  7.61 (d,  $J$ =8.4 Hz, 1H), 7.42 (d,  $J$ =8.1 Hz, 2 H), 7.08 (d,  $J$ =8.4 Hz, 2 H), 6.99 (s, 2 H), 6.93 (d,  $J$ =8.4 Hz, 2 H), 5.06 (s, 2 H), 4.15 (s, 1H), 2.52 (s, 2 H), 2.30–2.08 (m, 2 H), 1.05 (s, 3 H), 0.97 (s, 3 H).  $^{13}\text{C}$  NMR (76 MHz,  $\text{DMSO-}d_6$ )  $\delta$  196.26, 162.72, 158.90, 157.35, 137.71, 137.10, 131.83, 130.27, 128.73, 121.37, 120.30, 114.98, 113.38, 68.85, 58.95, 50.44, 35.20, 32.26, 28.84, 27.25. Ms m/z (%): 109.1(100), 90.2(16.5), 66.2(5.5), 217.2(7), 243.2(7), 281.1(3), 309.2(16.5), 414.2(5.5), 480.2(5.5), 478.2(5.5), 479.3(2), 481.2(1.5). IR (KBr,  $\text{cm}^{-1}$ )  $\nu$ : 3327.45 (N-H), 3216.72 (C-H aromatic), 2194.68(C $\equiv$ N), 1669 (C=O), 1599.43 (C=C aromatic), 1508.99 (C=C aromatic).

2-Amino-7,7-dimethyl-4-(4-((4-methylbenzyl)oxy)phenyl)-5-oxo-5,6,7,8-tetrahydro-4*H*-chromene-3-carbonitrile (6e).

White solid; Yield: 68%,  $R_f$ =0.42 (n-hexane: EtOAc (60:40)); mp: 222–223 °C.  $^1\text{H}$  NMR (301 MHz,  $\text{DMSO-}d_6$ )  $\delta$  7.34 (d,  $J$ =7.8 Hz, 2 H), 7.21 (d,  $J$ =7.7 Hz, 2 H), 7.07 (d,  $J$ =8.6 Hz, 2 H), 6.99 (s, 2 H), 6.96–6.90 (m, 2 H), 5.02 (s, 2 H), 4.14 (s, 1H), 2.52 (s, 2 H), 2.30–2.08 (m, 2 H), 1.05 (s, 3 H), 0.97 (s, 3 H).  $^{13}\text{C}$  NMR (76 MHz,  $\text{DMSO-}d_6$ )  $\delta$  196.18, 162.65, 158.89, 157.58, 137.52, 137.48, 134.58, 129.45, 128.69, 128.27, 120.30, 114.94, 113.43, 69.54, 58.97, 50.46, 35.21, 32.26, 28.85, 28.38, 27.27, 21.25. Ms m/z (%): 105.3(100), 77.3(7), 55.3(2), 161.2(2.5), 217.3(4.5), 243.3(2.5), 309.3(7), 348.3(4.5), 414.4(13.5). IR (KBr,  $\text{cm}^{-1}$ )  $\nu$ : 3323.18(N-H), 3211.77(C-H aromatic), 2190.45(C $\equiv$ N), 1659.26 (C=O), 1602.92 (C=C aromatic), 1507.66 (C=C aromatic).

2-Amino-4-(4-((4-cyanobenzyl)oxy)phenyl)-7,7-dimethyl-5-oxo-5,6,7,8-tetrahydro-4*H*-chromene-3-carbonitrile (**6f**).

White solid; Yield: 67%,  $R_f=0.41$  (n-hexane: EtOAc (60:40)); mp: 208–209 °C.  $^1\text{H NMR}$  (301 MHz,  $\text{DMSO-}d_6$ )  $\delta$  7.93–7.83 (m, 2 H), 7.65 (d,  $J=8.1$  Hz, 2 H), 7.13–7.06 (m, 2 H), 7.00 (s, 2 H), 6.98–6.86 (m, 2 H), 5.19 (s, 2 H), 4.15 (s, 1H), 2.53 (s, 2 H), 2.29–2.08 (m, 2 H), 1.05 (s, 3 H), 0.97 (s, 3 H).  $^{13}\text{C NMR}$  (76 MHz,  $\text{DMSO-}d_6$ )  $\delta$  196.18, 162.70, 158.88, 157.17, 143.51, 137.91, 132.91, 128.78, 128.54, 119.26, 114.99, 113.35, 110.90, 68.69, 35.20, 32.27, 28.85, 27.24. Ms m/z (%): 116.2(100), 89.2(16.5), 55.2(3.5), 159.2(11.5), 201.2(18.5), 243.3(56), 359.3(34), 285.1(3.5), 309.3(3.5), 359.3(35), 425.3(2), 262.1(2), 140.2(2) IR (KBr,  $\text{cm}^{-1}$ )  $\nu$ : 3330.14(N-H), 2186.44( $\text{C}\equiv\text{N}$ ), 1672.72( $\text{C}=\text{O}$ ), 1603.14( $\text{C}=\text{C}$  aromatic), 1509.36( $\text{C}=\text{C}$  aromatic).

2-Amino-4-(4-((4-chlorobenzyl)oxy)phenyl)-7,7-dimethyl-5-oxo-5,6,7,8-tetrahydro-4*H*-chromene-3-carbonitrile (**6g**).

White solid; Yield: 64%,  $R_f=0.45$  (n-hexane: EtOAc (60:40)); mp: 207–208 °C.  $^1\text{H NMR}$  (301 MHz,  $\text{DMSO-}d_6$ )  $\delta$  7.48 (s, 4H), 7.11–7.05 (m, 2 H), 6.99 (s, 2 H), 6.96–6.91 (m, 2 H), 5.07 (s, 2 H), 4.15 (s, 1H), 2.52 (s, 2 H), 2.30–2.08 (m, 2 H), 1.05 (s, 3 H), 0.97 (s, 3 H).  $^{13}\text{C NMR}$  (76 MHz,  $\text{DMSO-}d_6$ )  $\delta$  196.18, 162.67, 158.89, 157.37, 137.71, 136.68, 132.85, 129.97, 128.91, 128.74, 120.31, 114.96, 113.40, 68.80, 58.94, 50.45, 35.22, 32.25, 28.86, 27.25. Ms m/z (%): 125.1(100), 89.2(8), 66.2(4), 161.1(2), 217.2(7), 243.2(4), 281.1(2), 309.2(15), 368.2(5), 434.3(7.5) IR (KBr,  $\text{cm}^{-1}$ )  $\nu$ : 3323.22(N-H), 2194.57( $\text{C}\equiv\text{N}$ ), 1655.30( $\text{C}=\text{O}$ ), 1605.95 ( $\text{C}=\text{C}$  aromatic), 1507.92 ( $\text{C}=\text{C}$  aromatic).

2-Amino-4-(4-(benzyloxy)phenyl)-7,7-dimethyl-5-oxo-5,6,7,8-tetrahydro-4*H*-chromene-3-carbonitrile (**6h**).

White solid; Yield: 69%,  $R_f=0.57$  (n-hexane: EtOAc (60:40)); mp: 221–222 °C.  $^1\text{H NMR}$  (301 MHz,  $\text{DMSO-}d_6$ )  $\delta$  7.47–7.40 (m, 5 H), 7.22–7.16 (m, 2 H), 6.96–6.90 (m, 2 H), 5.05 (s, 2 H), 4.63 (d,  $J=20.9$  Hz, 2 H), 4.40 (s, 1H), 2.48 (s, 2 H), 2.26 (d,  $J=2.8$  Hz, 2 H), 1.14 (s, 3 H), 1.07 (s, 3 H).  $^{13}\text{C NMR}$  (76 MHz,  $\text{DMSO-}d_6$ )  $\delta$  196.09, 161.36, 157.96, 157.45, 137.09, 135.77, 128.69, 128.61, 127.98, 127.64, 127.58, 118.84, 114.88, 114.24, 77.26, 70.04, 63.72, 50.71, 40.69, 34.77, 32.23, 28.89, 27.73. Ms m/z (%): 91.2(100), 65.2(33.5), 112.2(20), 140.2(26), 217.2(4), 169.1(3.5), 243.2(7), 260.1(20), 309.2(8.5), 334.3(8), 400.3(6.5) IR (KBr,  $\text{cm}^{-1}$ )  $\nu$ : 3323.18(N-H), 3210.66( $\text{C-H}$  aromatic), 2187.16( $\text{C}\equiv\text{N}$ ), 1659.30 ( $\text{C}=\text{O}$ ), 1603.04( $\text{C}=\text{C}$  aromatic), 1508.73 ( $\text{C}=\text{C}$  aromatic).

2-Amino-4-(4-((3-fluorobenzyl)oxy)-3-methoxyphenyl)-7,7-dimethyl-5-oxo-5,6,7,8-tetrahydro-4*H*-chromene-3-carbonitrile (**6i**).

White solid; Yield: 58%,  $R_f=0.52$  (n-hexane: EtOAc (60:40)); mp:174–175 °C.  $^1\text{H NMR}$  (301 MHz,  $\text{DMSO-}d_6$ )  $\delta$  7.49–7.42 (m, 1H), 7.32–7.25 (m, 2 H), 7.18 (td,  $J=7.3$ , 1.7 Hz, 1H), 6.99 (s, 2 H), 6.96 (d,  $J=8.3$  Hz, 1H), 6.75 (d,  $J=2.1$  Hz, 1H), 6.66 (dd,  $J=8.2$ , 2.1 Hz, 1H), 5.08 (s, 2 H), 4.15 (s, 1H), 3.76 (s, 3 H), 2.54 (s, 2 H), 2.31–2.11 (m, 2 H), 1.06 (s, 3 H), 1.00 (s, 3 H).  $^{13}\text{C NMR}$  (76 MHz,  $\text{DMSO-}d_6$ )  $\delta$  196.22, 162.86, 158.85, 149.25, 146.82, 140.75, 138.44, 130.98, 130.87, 124.05, 120.30, 119.53, 115.17, 114.87, 114.58, 113.99, 113.20, 111.69, 69.60, 58.87, 55.99, 50.44, 35.51, 32.24, 28.96, 27.11. Ms m/z (%): 109.2(100), 83.2(22.5), 55.2(4.5), 161.2(8.5), 189.2(8.5), 231.2(14.5), 273.3(76.5), 311.3(13.3), 339.3(34.5), 382.3(46.5), 448.3(15), 449.3(4.5) IR (KBr,  $\text{cm}^{-1}$ )  $\nu$ : 314.49(N-H), 3190.11( $\text{C-H}$  aromatic), 2191.59( $\text{C}\equiv\text{N}$ ), 1655.30( $\text{C}=\text{O}$ ), 1607.68( $\text{C}=\text{C}$  aromatic), 1514.57 ( $\text{C}=\text{C}$  aromatic).

2-Amino-4-(4-((2-fluorobenzyl)oxy)-3-methoxyphenyl)-7,7-dimethyl-5-oxo-5,6,7,8-tetrahydro-4*H*-chromene-3-carbonitrile (**6j**).

White solid; Yield: 56%,  $R_f=0.52$  (n-hexane: EtOAc (60:40)); mp: 200–201 °C.  $^1\text{H NMR}$  (301 MHz,  $\text{DMSO-}d_6$ )  $\delta$  7.56 (td,  $J=7.5$ , 1.7 Hz, 1H), 7.44 (dtd,  $J=7.4$ , 6.4, 1.9 Hz, 1H), 7.27 (tdd,  $J=7.5$ , 5.6, 1.3 Hz, 2 H), 7.03 (s, 1H), 7.00 (d,  $J=2.6$  Hz, 2 H), 6.74 (d,  $J=2.1$  Hz, 1H), 6.68 (dd,  $J=8.2$ , 2.1 Hz, 1H), 5.08 (s, 2 H), 4.16 (s, 1H), 3.73 (s, 3 H), 2.55 (s, 2 H), 2.32–2.10 (m, 2 H), 1.06 (s, 3 H), 1.00 (s, 3 H).  $^{13}\text{C NMR}$  (76 MHz,  $\text{DMSO-}d_6$ )  $\delta$  196.21, 162.85, 162.49, 159.23, 158.86, 149.21, 146.88, 138.48, 131.35, 131.30, 130.91, 130.80, 125.02, 124.98, 124.54, 124.34, 120.29, 119.56, 115.97, 115.69, 113.81, 113.22, 111.71, 64.60, 63.84, 58.88, 55.93, 50.46, 35.52, 32.23, 28.97, 27.11. Ms m/z (%): 109.2(100), 83.2(18), 55.2(3.5), 140.2(3), 161.2(5), 189.2(5), 217.2(8), 245.3(4), 273.3(31), 339.3(12), 308.2(4) 382.3(31), 448.3(4), 449.3(2) IR (KBr,  $\text{cm}^{-1}$ )  $\nu$ : 3317.34(N-H), 3208.57( $\text{C-H}$  aromatic), 2191.17( $\text{C}\equiv\text{N}$ ), 1653.42( $\text{C}=\text{O}$ ), 1606.69( $\text{C}=\text{C}$  aromatic), 1514.78 ( $\text{C}=\text{C}$  aromatic).

2-Amino-4-(4-((4-fluorobenzyl)oxy)-3-methoxyphenyl)-7,7-dimethyl-5-oxo-5,6,7,8-tetrahydro-4*H*-chromene-3-carbonitrile (**6k**).

White solid; Yield: 58%,  $R_f=0.52$  (n-hexane: EtOAc (60:40)); mp: 184–186 °C.  $^1\text{H NMR}$  (301 MHz,  $\text{DMSO-}d_6$ )  $\delta$  7.54–7.46 (m, 2 H), 7.29–7.20 (m, 2 H), 6.99 (s, 2 H), 6.96 (s, 1H), 6.74 (d,  $J=2.0$  Hz, 1H), 6.66 (dd,  $J=8.2$ , 2.1 Hz, 1H), 5.03 (s, 2 H), 4.15 (s, 1H), 3.74 (s, 3 H), 2.55 (s, 2 H), 2.32–2.11 (m, 2 H), 1.06 (s, 3 H), 1.00 (s, 3 H).  $^{13}\text{C NMR}$  (76 MHz,  $\text{DMSO-}d_6$ )  $\delta$  196.22, 163.85, 162.85, 160.62, 158.86, 149.24, 146.95, 138.30, 133.95, 133.91, 131.81, 130.54, 130.43, 120.29, 119.52, 115.83, 115.55, 113.93, 113.23, 111.68, 69.70, 58.92, 55.96, 50.45, 35.51, 32.23, 28.96, 27.10. Ms m/z (%): 109.2(100), 83.2(12.5), 55.2(3.5), 140.2(2), 161.1(3), 189.1(1.5), 217.2(11), 245.2(1.5),

273.1(3.5), 311.2(6), 339.2(16), 382.3(10), 448.3(6) IR (KBr,  $\text{cm}^{-1}$ )  $\nu$ : 3324.67(N-H), 3210.39(C-H aromatic), 2194.46(C $\equiv$ N), 1649.40(C=O), 1603.53(C=C aromatic), 1507.18(C=C aromatic).

2-Amino-4-(4-((4-bromobenzyl)oxy)-3-methoxyphenyl)-7,7-dimethyl-5-oxo-5,6,7,8-tetrahydro-4H-chromene-3-carbonitrile (**6L**).

White solid; Yield: 63%,  $R_f$ =0.52 (n-hexane: EtOAc (60:40)); mp: 197–198 °C.  $^1\text{H}$  NMR (301 MHz, DMSO- $d_6$ )  $\delta$  7.61 (d,  $J$ =8.3 Hz, 1H), 7.41 (d,  $J$ =8.4 Hz, 1H), 6.99 (s, 2 H), 6.95 (d,  $J$ =8.3 Hz, 1H), 6.74 (d,  $J$ =2.1 Hz, 1H), 6.65 (dd,  $J$ =8.2, 2.1 Hz, 1H), 5.03 (s, 2 H), 4.15 (s, 1H), 3.74 (s, 3 H), 2.54 (s, 2 H), 2.31–2.10 (m, 2 H), 1.06 (s, 3 H), 1.00 (s, 3 H).  $^{13}\text{C}$  NMR (76 MHz, DMSO- $d_6$ )  $\delta$  196.23, 162.87, 158.86, 149.23, 146.84, 138.38, 137.20, 131.81, 130.32, 121.38, 120.30, 119.51, 113.97, 113.21, 111.68, 69.61, 58.89, 55.97, 50.44, 35.50, 32.23, 28.96, 27.11. Ms m/z (%): 169.2(100), 90.2(15.5), 55.2(4.5), 146.2(2), 115.2(2), 191.2(3), 231.2(6.5), 273.3(44.5), 442.2(24.5) IR (KBr,  $\text{cm}^{-1}$ )  $\nu$ : 3316.38(N-H), 2202.25(C $\equiv$ N), 1654.32(C=O), 1514.89(C=C aromatic).

2-Amino-4-(3-methoxy-4-((4-methylbenzyl)oxy)phenyl)-7,7-dimethyl-5-oxo-5,6,7,8-tetrahydro-4H-chromene-3-carbonitrile (**6m**).

White solid; Yield: 62%,  $R_f$ =0.52 (n-hexane: EtOAc (60:40)); mp: 180–182 °C.  $^1\text{H}$  NMR (301 MHz, DMSO- $d_6$ )  $\delta$  7.36–7.31 (m, 2 H), 7.21 (d,  $J$ =7.8 Hz, 2 H), 6.99 (s, 2 H), 6.96 (d,  $J$ =8.3 Hz, 1H), 6.73 (d,  $J$ =2.1 Hz, 1H), 6.65 (dd,  $J$ =8.3, 2.1 Hz, 1H), 4.99 (s, 2 H), 4.15 (s, 1H), 3.73 (s, 3 H), 2.52 (s, 2 H), 2.31–2.10 (m, 2 H), 1.06 (s, 3 H), 1.00 (s, 3 H).  $^{13}\text{C}$  NMR (76 MHz, DMSO- $d_6$ )  $\delta$  196.20, 162.83, 158.86, 149.21, 147.10, 138.08, 137.52, 134.65, 129.42, 128.38, 120.30, 119.52, 113.79, 113.25, 111.67, 70.27, 58.93, 55.96, 50.46, 35.49, 32.23, 28.96, 27.13, 21.25. Ms m/z (%): 105.2(100), 77.2(5), 55.2(2.5), 273.1(5), 378.3(14) IR (KBr,  $\text{cm}^{-1}$ )  $\nu$ : 3323.93(N-H), 2194.48(C $\equiv$ N), 1652.29(C=O), 1602.64(C=C aromatic), 1503.82 (C=C aromatic).

2-Amino-4-(4-((4-chlorobenzyl)oxy)-3-methoxyphenyl)-7,7-dimethyl-5-oxo-5,6,7,8-tetrahydro-4H-chromene-3-carbonitrile (**6n**).

White solid; Yield: 60%,  $R_f$ =0.55 (n-hexane: EtOAc (60:40)); mp: 194–195 °C.  $^1\text{H}$  NMR (301 MHz, DMSO- $d_6$ )  $\delta$  7.47 (s, 4H), 6.99 (s, 2 H), 6.95 (d,  $J$ =8.2 Hz, 1H), 6.74 (d,  $J$ =2.0 Hz, 1H), 6.65 (dd,  $J$ =8.2, 2.1 Hz, 1H), 5.05 (s, 2 H), 4.15 (s, 1H), 3.74 (s, 3 H), 2.54 (s, 2 H), 2.31–2.10 (m, 2 H), 1.06 (s, 3 H), 1.00 (s, 3 H).  $^{13}\text{C}$  NMR (76 MHz, DMSO- $d_6$ )  $\delta$  196.21, 162.86, 158.86, 149.25, 146.86, 136.79, 132.83, 130.02, 128.89, 119.51, 113.99, 113.21, 111.70, 69.59, 58.90, 55.98, 50.44, 35.50, 32.23, 28.96, 27.12. Ms m/z (%): 125.2(100), 83.2(10), 55.2(3.5), 161.2(2), 189.2(2),

231.2(3), 273.3(16.5), 324.2(2), 398.3(12). IR (KBr,  $\text{cm}^{-1}$ )  $\nu$ : 3317.91(N-H), 3189.90(C-H aromatic), 2203.94(C $\equiv$ N), 1654.44(C=O), 1607.68(C=C 1514.70 (C=C aromatic).

2-Amino-4-(4-(benzyloxy)-3-methoxyphenyl)-7,7-dimethyl-5-oxo-5,6,7,8-tetrahydro-4H-chromene-3-carbonitrile (**6o**).

White solid; Yield: 64%,  $R_f$ =0.50 (n-hexane: EtOAc (60:40)); mp: 224–226 °C.  $^1\text{H}$  NMR (301 MHz, DMSO- $d_6$ )  $\delta$  7.48–7.34 (m, 5 H), 6.99 (d,  $J$ =1.9 Hz, 2 H), 6.96 (s, 1H), 6.74 (d,  $J$ =2.1 Hz, 1H), 6.66 (dd,  $J$ =8.2, 2.1 Hz, 1H), 5.05 (s, 2 H), 4.16 (s, 1H), 3.74 (s, 3 H), 2.54 (s, 2 H), 2.32–2.10 (m, 2 H), 1.06 (s, 3 H), 1.00 (s, 3 H).  $^{13}\text{C}$  NMR (76 MHz, DMSO- $d_6$ )  $\delta$  196.22, 162.85, 158.86, 149.22, 147.08, 138.18, 137.69, 128.88, 128.29, 120.31, 119.53, 113.80, 113.24, 111.66, 70.40, 58.93, 55.96, 50.46, 35.51, 32.24, 28.97, 27.12. Ms m/z (%): 91.2(100), 65.2(6), 161.2(5.5), 133.2(2.5), 189.2(2.5), 217.3(19.5), 245.2(2.5), 273.3(23), 311.3(11.5), 339.3(29), 364.3(24), 430.3(15) IR (KBr,  $\text{cm}^{-1}$ )  $\nu$ : 3314.58(N-H), 3192.12(C-H aromatic), 2191.41(C $\equiv$ N), 1653.93(C=O), 1608.17(C=C aromatic), 1514.90 (C=C aromatic).

#### **In vitro tyrosinase inhibition assay**

We modified a previously described method [19] to conduct the mushroom tyrosinase (EC 1.14.18.1) assay using *L*-Dopa as the substrate. To measure the enzyme's diphenolase activity, we employed a spectrophotometric approach to monitor the production of dopachrome at 490 nm. All compounds being evaluated, including kojic acid, were dissolved in dimethyl sulfoxide (DMSO- $d_6$ ) and then diluted to the desired concentrations. In a 96-well microplate, 10  $\mu\text{l}$  ( $\mu\text{l}$ ) of each sample was combined with 160  $\mu\text{l}$  of 50 millimolar (mM) phosphate buffer at a pH of 6.8. Next, 10  $\mu\text{l}$  of tyrosinase (at a concentration of 600 U  $\text{mL}^{-1}$ ) was added [35]. After a 20-minute pre-incubation period at 28 °C, 20  $\mu\text{l}$  of *L*-Dopa solution was introduced, achieving a final concentration of 0.7 mM. After an additional 10-minute incubation period, the absorbance was recorded. The inhibitory activity of the compounds was expressed as  $\text{IC}_{50}$  values, which represent the concentration required to inhibit 50% of the maximum response.

The percentage inhibition was calculated using the following equation:

$$\text{Inhibition (\%)} = 100 (\text{Abs}_{\text{control}} - \text{Abs}_{\text{compound}}) / \text{Abs}_{\text{control}}$$

#### **Determination of the inhibition type**

To conduct the kinetic analysis, we focused on compound **6f**, which was identified as the most effective derivative. The inhibitor concentrations ranged from 5 to 50  $\mu\text{M}$ , while the substrate (*L*-Dopa) concentrations ranged from 0.1 mM to 1.5 mM in all kinetic experiments. We followed the pre-incubation and measurement durations

outlined in the mushroom tyrosinase inhibition assay protocol [4]. The maximum initial velocity was determined from the initial linear segment of absorbance within a 10-minute window after adding *L*-Dopa, with measurements taken at 1-minute intervals. The Michaelis constant ( $K_m$ ) and the maximum velocity ( $V_{max}$ ) of tyrosinase activity were calculated using the Lineweaver–Burk plot method, which involved varying concentrations of *L*-Dopa as the substrate. To determine the type of enzyme inhibition, we utilized Lineweaver–Burk plots that displayed the reciprocal of velocities ( $1/V$ ) against the reciprocal of substrate concentrations ( $1/[S]$   $\text{mM}^{-1}$ ) [36].

#### Drug-likeness, ADMET properties and PAINS filters: in silico prediction

The parameters for the selected compounds (**6e** and **6f**), including the number of hydrogen bond acceptors (HBA) and donors (HBD), logP values, topological polar surface area (tPSA), and the count of rotatable bonds (RBC), were determined utilizing the online tools SwissADME and pkCSM [27, 28, 37]. Additionally, the ADMET properties of these compounds were evaluated through the pkCSM software and ProTox online servers. Also, The Pan-Assay Interference Compounds (PAINS) screening was conducted using the SwissADME tool and further validated with the “False Positive Remover” software (<http://www.cbligand.org/PAINS/>) [38].

#### Docking study

The crystallographic structure of tyrosinase enzyme (PDB ID: 2Y9X) with a resolution of 2.78 Å was obtained from the RCSB Protein Data Bank. The 3D structure of compound **6f** was optimized using density functional theory (DFT) with the BP86/DEF2-TZVP basis set in the ORCA quantum chemistry package [39]. Rigid-ligand molecular docking studies of the R and S enantiomers of **6f** were performed using AutoDock Tools 1.5.4 (ADT) [40].

For the preparation of the enzyme, water molecules and other non-essential components were removed from the enzyme's structure. Hydrogen atoms were added, and non-polar hydrogens were merged with their corresponding carbon atoms. Kollman partial atomic charges were assigned using ADT. An AutoGrid calculation generated a grid map, with the grid box centered at coordinates  $x = -30.194$ ,  $y = -4.738$ , and  $z = -93.823$ . The cubic box size was  $60 \times 60 \times 60$ , featuring a grid spacing of 0.375 Å. Docking simulations were conducted utilizing the Lamarckian genetic algorithm, which began with a population size of 150, a maximum number of evaluations of 25,000,000, a maximum number of generations of 27,000, and 100 independent runs.

#### MD simulations

Molecular dynamics simulations were conducted using the Desmond v5.3 module within the Maestro interface from the Schrödinger 2018–4 suite [41]. The optimal pose for the molecular dynamics simulation of compound **6f** was determined through the IFD method. The system was prepared by solvating the protein-ligand complex with explicit water molecules, and counter-ions, along with NaCl were added to achieve cellular ionic concentrations.

The molecular dynamics protocol included minimization, pre-production, and production molecular dynamics steps. The simulations were performed in the NPT ensemble, which maintains a constant number of particles (N), pressure (P), and temperature (T) throughout the simulation. The system underwent a 100 ns molecular dynamics simulation, during which the dynamic behavior and structural changes were analyzed using the root mean square deviation (RMSD). Additionally, protein-ligand interactions were investigated using the energy-minimized structure from the equilibrated trajectory [10, 12].

#### Supplementary Information

The online version contains supplementary material available at <https://doi.org/10.1186/s13065-024-01305-0>.

Supplementary Material 1

#### Acknowledgements

The authors of this article would like to thank the Vice-Chancellor of Research and Technology of Hamedan University of Medical Sciences and the Vice-Chancellor for Research of Shiraz University of Medical Sciences for the financial support of this research.

#### Author contributions

AB and MA synthesized all compounds. MA wrote the draft of the manuscript. AI performed molecular dynamics and anti-tyrosinase study and edited the manuscript. ZN was the scientific advisor of this research. GC designed, analyzed, and edited the manuscript.

#### Funding

Funds for this study were provided by the Research and Technology Vice-chancellor of Hamadan University of Medical Sciences (Grant Number: IR.SUMS.REC.1403.205) related to Azimi's thesis and the Vice-Chancellor for Research of Shiraz University of Medical Sciences (Grant Number: 31285).

#### Data availability

No datasets were generated or analysed during the current study.

#### Declarations

##### Ethics approval and consent to participate

Not applicable.

##### Consent for publication

Not applicable.

##### Competing interests

The authors declare no competing interests.

Published online: 28 September 2024

## References

- Li J, et al. Recent advances in the design and discovery of synthetic tyrosinase inhibitors. *Eur J Med Chem.* 2021;224:113744.
- Choi YJ, et al. Synthesis and biological evaluation of kojic acid derivatives as tyrosinase inhibitors. *Bull Korean Chem Soc.* 2014;35(12):3647–50.
- Alizadeh N, et al. Evaluating the effects of disubstituted 3-hydroxy-1H-pyrrol-2 (5H)-one analog as novel tyrosinase inhibitors. *Bioorg Chem.* 2022;126:105876.
- Hosseinpoor H, et al. Anti-melanogenesis and anti-tyrosinase properties of aryl-substituted acetamides of phenoxy methyl triazole conjugated with thiosemicarbazide: design, synthesis and biological evaluations. *Bioorg Chem.* 2021;114:104979.
- Solano F. On the metal cofactor in the tyrosinase family. *Int J Mol Sci.* 2018;19(2):633.
- Obaid RJ, et al. Natural and synthetic flavonoid derivatives as new potential tyrosinase inhibitors: a systematic review. *RSC Adv.* 2021;11(36):22159–98.
- Pillaiyar T, Manickam M, Namasivayam V. Skin whitening agents: Medicinal chemistry perspective of tyrosinase inhibitors. *J Enzyme Inhib Med Chem.* 2017;32(1):403–25.
- Sepehri N, et al. The natural-based optimization of kojic acid conjugated to different thio-quinazolinones as potential anti-melanogenesis agents with tyrosinase inhibitory activity. *Bioorg Med Chem.* 2021;36:116044.
- Hashemi A, et al. Synthesis and tyrosinase inhibitory activities of novel isopropylquinazolinones. *BMC Chem.* 2023;17(1):65.
- Iraji A, et al. Design, synthesis, spectroscopic characterization, in vitro tyrosinase inhibition, antioxidant evaluation, in silico and kinetic studies of substituted indole-carbohydrazides. *Bioorg Chem.* 2022;129:106140.
- Ullah S, et al. Tyrosinase inhibitors: a patent review (2011–2015). *Expert Opin Ther Pat.* 2016;26(3):347–62.
- Ghasemi N, et al. Thiazolopyrimidine derivatives as novel class of small molecule tyrosinase inhibitor. *BMC Chem.* 2023;17(1):156.
- Iraji A, et al. Synthesis, biological evaluation and molecular docking analysis of vaniline-benzylidenehydrazine hybrids as potent tyrosinase inhibitors. *BMC Chem.* 2020;14(1):1–11.
- Saeedi M, Eslamifard M, Khezri K. Kojic acid applications in cosmetic and pharmaceutical preparations. *Biomed Pharmacother.* 2019;110:582–93.
- Rezapour Niri D et al. Design, synthesis, in vitro, and in silico evaluations of kojic acid derivatives linked to amino pyridine moiety as potent tyrosinase inhibitors. *Heliyon.* 2023;9(11).
- Kang SS, et al. Synthesis of tyrosinase inhibitory (4-oxo-4H-pyran-2-yl) acrylic acid ester derivatives. *Bioorg Med Chem Lett.* 2009;19(1):188–91.
- Debbabi M, et al. Design and synthesis of novel potent anticoagulant and anti-tyrosinase pyranopyrimidines and pyranotriazolopyrimidines: insights from molecular docking and SAR analysis. *Bioorg Chem.* 2019;82:129–38.
- Wang Y, et al. Inhibition of tyrosinase activity by polyphenol compounds from *Flemingia philippinensis* roots. *Bioorg Med Chem.* 2014;22(3):1115–20.
- Najafi Z, et al. Design, synthesis, and molecular dynamics simulation studies of some novel kojic acid fused 2-amino-3-cyano-4H-pyran derivatives as tyrosinase inhibitors. *BMC Chem.* 2024;18(1):41.
- Babae S, et al. Design, synthesis, and Molecular Docking of some Novel Tacrine based cyclopentapyranopyridine-and tetrahydropranoquinoline-Kojic acid derivatives as anti-acetylcholinesterase agents. *Chem Biodivers.* 2021;18(6):e2000924.
- Sadafi Kohnehshahri M et al. Novel tacrine-based acetylcholinesterase inhibitors as potential agents for the treatment of Alzheimer's disease: quinolotacrines hybrids. *Mol Divers.* 2022;26:1–15.
- Ebadi A, et al. Novel Xanthene-1, 8-dione derivatives containing the Benzylic Ether tail as potent cytotoxic agents: design, synthesis, in Vitro, and in Silico studies. *J Chem.* 2024;2024(1):6612503.
- Najafi Z, et al. Synthesis and molecular modeling of new 2-benzylidene-thio-barbituric acid derivatives as potent tyrosinase inhibitors agents. *J Chin Chem Soc.* 2022;69(4):692–702.
- Najafi Z, et al. Design, synthesis, in vitro, and in silico studies of novel benzylidene 6-methoxy-1-tetralone linked to benzyloxy and benzyl-1, 2, 3-triazole rings as potential tyrosinase inhibitors. *J Mol Struct.* 2023;1271:134018.
- Ismaya WT, et al. Crystal structure of *Agaricus Bisporus* mushroom tyrosinase: identity of the tetramer subunits and interaction with tropolone. *Biochem.* 2011;50(24):5477–86.
- Lipinski CA, et al. Experimental and computational approaches to estimate solubility and permeability in drug discovery and development settings. *Adv Drug Deliv Rev.* 1997;23(1–3):3–25.
- Daina A, Michielin O, Zoete V. SwissADME: a free web tool to evaluate pharmacokinetics, drug-likeness and medicinal chemistry friendliness of small molecules. *Sci Rep.* 2017;7(1):42717.
- Pires DE, Blundell TL, Ascher DB. pkCSM: predicting small-molecule pharmacokinetic and toxicity properties using graph-based signatures. *J Med Chem.* 2015;58(9):4066–72.
- Banerjee P et al. ProTox 3.0: a webserver for the prediction of toxicity of chemicals. *Nucleic Acids Res.* 2024;52:gkae303.
- Sidhom PA, et al. Mechanistic insight of synthesized 1,4-Dihydropyridines as an Antidiabetic Sword against reactive oxygen species. *J Med Chem.* 2023;66(1):991–1010.
- Sidhom PA, et al. Revisiting ageless antiques; synthesis, biological evaluation, docking simulation and mechanistic insights of 1, 4-Dihydropyridines as anticancer agents. *Bioorg Chem.* 2021;114:105054.
- Jasial S, Hu Y, Bajorath Jr. How frequently are pan-assay interference compounds active? Large-scale analysis of screening data reveals diverse activity profiles, low global hit frequency, and many consistently inactive compounds. *J Med Chem.* 2017;60(9):3879–86.
- Sidhom PA, et al. Mechanistic insight of synthesized 1, 4-dihydropyridines as an antidiabetic sword against reactive oxygen species. *J Med Chem.* 2022;66(1):991–1010.
- Ebadi A, et al. Design, synthesis, molecular modeling and DNA-binding studies of new barbituric acid derivatives. *J Iran Chem Soc.* 2022;19(9):3887–98.
- Iraji A, et al. Synthesis, biological evaluation and molecular docking analysis of vaniline-benzylidenehydrazine hybrids as potent tyrosinase inhibitors. *BMC Chem.* 2020;14(1):28.
- Hosseinpoor H, et al. A series of Benzylidenes Linked to Hydrazine-1-carbothioamide as tyrosinase inhibitors: synthesis, Biological evaluation and structure-activity relationship. *Chem Biodivers.* 2020;17(8):e2000285.
- Hussein HY, et al. Novel pyrazoline-thiazole hybrids containing azo group as antibacterial agents: design, synthesis, in vitro bioactivity, in silico molecular docking, ADME profile and DFT studies. *Res Chem Intermed.* 2024;50(9):4551–78.
- Bogoyavlenskii A, et al. Naturally occurring isorhamnetin glycosides as potential agents against Influenza viruses: antiviral and molecular Docking studies. *ACS Omega.* 2023;8(50):48499–514.
- Neese F. The ORCA program system. *Wiley Interdiscip Rev Comput Mol Sci.* 2012;2(1):73–8.
- Morris GM, et al. AutoDock4 and AutoDockTools4: automated docking with selective receptor flexibility. *J Comput Chem.* 2009;30(16):2785–91.
- Chinnasamy S, et al. Molecular docking and molecular dynamics simulation studies to identify potent AURKA inhibitors: assessing the performance of density functional theory, MM-GBSA and mass action kinetics calculations. *J Biomol Struct Dyn.* 2020;38(14):4325–35.

## Publisher's note

Springer Nature remains neutral with regard to jurisdictional claims in published maps and institutional affiliations.